Comparison between two multicomponent drug delivery systems based on PEGylated-poly (L-lactide-co-glycolide) and superparamagnetic nanoparticles: Nanoparticulate versus nanocluster systems

Comparison between two multicomponent drug delivery systems based on PEGylated-poly (L-lactide-co-glycolide) and superparamagnetic nanoparticles: Nanoparticulate versus nanocluster systems

Alma Lucia Villela Zumaya[a], Pavel Ulbrich[b], Jarmila Vilčáková[c], Marcela Dendisová[a], Michal Fulem[a], Miroslav Šoóš[a], Fatima Hassouna[a]

[a]*Faculty of Chemical Engineering, University of Chemistry and Technology, Prague, 166 28, Prague 6, Czech Republic*

[b]*Department of Biochemistry and Microbiology, University of Chemistry and Technology, Prague, 166 28, Prague 6, Czech Republic c Centre of Polymer Systems, Tomas Bata University, 760 01, Zlin, Czech Republic*

[*]*Corresponding author: E-mail address: fatima.hassouna@vscht.cz (F. Hassouna)*

ABSTRACT

Development of versatile and efficient multicomponent drug delivery nanocarriers in the range of hundreds of nanometers in size with tunable surface properties presents an interesting platform for biomedical applications. In this study, two approaches were evaluated for preparation of multi-component drug delivery nanocarriers based on the assembly of drug loaded PEGylated poly(L-lactide-co-glycolide) nanoparticles (PEGylated PLGA NPs) and superparamagnetic iron oxide nanoparticles (IO NPs). In the first approach, preparation of nanoclusters was performed by self-assembly of oppositely charged ibuprofen loaded PEGylated-PLGA and IO NPs, while in the second one IO NPs and a model drug (ibuprofen) were incorporated inside PEGylated PLGA NPs by single emulsion method. Nanoclusters as well as multi-component loaded PEGylated PLGA NPs with a size of 350 ± 71 nm and 238 ± 88 nm, respectively, were produced. Interestingly, both delivery systems demonstrated comparable drug release behavior after 120 h. They exhibited also comparable magnetic properties before and after dissolution tests. Mechanistic insights into the effect of the morphology and chemical composition of the multicomponent delivery systems on the drug release mechanisms are proposed.

Keywords: PEGylated-PLGA nanoparticles, iron oxide nanoparticles, multicomponent drug delivery, nanoclusters, drug release kinetics, magnetic properties

1. Introduction

Nanomaterial systems have become increasingly important in medicine due to their unique physical properties as they can act as drug vehicles, theragnostics and therapeutic systems [**1**]. In the last decades, polymeric and superparamagnetic nanoparticles have gained importance for the development of efficient drug delivery systems towards cancer treatment [**2,3**]. The incorporation of polymeric nanocarriers can enhance bioavailability of poorly water soluble drugs and organ or cell-specific drug accumulation. This enables the design of drug delivery systems with controlled drug release to the targeted sites, e.g. cancer cells [**2**]. Various biocompatible materials exhibiting low toxicity have been employed to prepare particles with sizes ranging from 20 to 1000 nm such as chitosan, gelatin, alginate, poly (e-caprolactone) (PCL), poly (lactide) (PLA) and poly(lactide-co-

glycolide) (PLGA) [**4,5**]. The chemical structure, physico-chemical and rheological properties of the polymer determine also if it is suitable to carry hydrophobic or hydrophilic drugs and affect the rate and the profile of the drug release since this is controlled by polymer degradation kinetics, which can be induced either by hydrolysis or enzymatic degradation [**6**]. In spite of the afore-mentioned tremendous advances made in drug delivery using nanoparticles, the delivery of a single therapeutic agent can reach its limits in terms of prevention of disease relapsing [**7**]. With this respect, a strategy consisting of administration of multicomponent delivery system with multi-functionalities would be more beneficial as it is expected to substantially increase the efficiency of the treatment [**8**]. The association of multiple functionalities may include drug delivery, targeting, imaging, magnetic hyperthermia and radiotherapeutics. The benefits of employing a multicomponent system include the cytotoxicity decrease in the body, the possibility to reduce the chemotherapeutic drug dose and improvement of the pharmacokinetic profiles [**9,10**]. The most versatile way consists of combining various components with various functionalities within a single particle [**8,9,11-13**]. Although this approach offers numerous advantages, it often necessitates the utilization of unfriendly chemicals that may come in contact with the entrapped biomolecules, resulting in a loss of the bioactivity of the drug [**14**]. In this regard, we have recently developed a simple and versatile approach based on self-assembly of oppositely charged polymeric and inorganic nanoparticles via electrostatic interactions to construct nanoclusters with a size in a range of hundreds of nanometers for controlled drug delivery [**15**]. The nanoclusters prepared by self-assembly of the oppositely charged drug loaded PLGA nanoparticles (PLGA NPs) and superparamagnetic iron oxide nanoparticles (IO NPs) displayed a faster drug release in comparison with PLGA NPs after 24 h. The faster degradation of PLGA matrix in the presence of magnetic nanoparticles was related to the catalytic activity of the latter. The preservation of the magnetic properties of the nanoclusters after the dissolution tests was shown. This gives the possibility to the nanoclusters to be used for magnetic hyperthermia [**16**], even after the drug release. Indeed, IO NPs possess high contrast and superparamagnetic properties that are used for diagnosis and targeted delivery using magnetic field and for inducing local heating of the tumor by magnetic hyperthermia [**17,18**]. In addition, IO NPs present in the clusters can act as a magnetic resonance contrast agent. Thereby, the conservation of their magnetic properties subsequently to the drug release is beneficial. PLGA used for the preparation of the nanoclusters exhibit attractive features for the delivery of proteins, drugs, and other macromolecules, as the degradation rate of the polymer in the body via hydrolysis can be well-controlled. It can be also triggered by change in pH or temperature [**19**]. The degradation rate of the matrix can be controlled by the adjustment of the molar ratio between lactide and glycolide and the molecular weight of the copolymer during the polymerization [**20**]. Nevertheless, PLGA NPs present some disadvantages as the nanoparticles partake in the recognition by the reticulo-endothelial system (RES) of the spleen and liver as well as the necessity to employ a non-compatible stabilizer to obtain a small diameter with uniform distribution [**21**]. In addition, their short circulation time limits their capacity to attain the targeted cells and their efficacy [**22**]. In this regard, introduction of poly(ethylene glycol) (PEG) on the surface of the PLGA NPs, or PEGylation, gives them stealth properties by forming a hydrophilic steric barrier that delays opsonization and fast recognition by the RES [**23**]. PEGylation of PLGA NPs also confers colloidal stability and thus reduces intermolecular aggregation through inter-particle steric repulsion [**24,25**].

By combining multiple components and functionalities into a single drug delivery system, in a form of either multicomponent single nanoparticle or nanocluster, a proper control of the surface functionalization of the polymeric nanoparticles should allow tailoring the performance of the system [**26,27**]. Hence, the goal of this study was to develop and compare the performance of two multicomponent drug delivery nanocarriers with multi-functionalities in the range of hundreds of nanometers in diameter. They were elaborated from PEGylated-PLGA NPs, model drug and

superparamagnetic IO NPs. Assembly of the components composing the drug delivery nanocarriers was achieved using two main approaches. In one approach, preparation of nanoclusters was done by self-assembly of oppositely charged nanoparticles, i.e., drug loaded PEGylated-PLGA NPs and IO NPs [**15**] while in the second one, IO NPs and a model drug were incorporated inside PEGylated-PLGA NPs. For this, aqueous and organic IO NPs were synthesized by co-precipitation method. In addition, low molecular weight NH_2-terminated PEG-PLGA copolymer was synthesized to prepare PEGylated PLGA NPs. Characterization of the IO NPs, PLGA-PEG-NH2 copolymer and its resulting nanoparticles, multicomponent drug delivery carriers (i.e. nanoclusters and multi-component loaded PEGylated-PLGA NPs) was carried out by studying the chemical structure, physico-chemical properties, morphology, particle size, size distribution, zeta potential and the magnetic properties. Furthermore, drug release kinetics of the two types of multicomponent delivery carriers were investigated and compared. This study allowed to generate fundamental understanding of relationships between the process of material preparation and their delivery behavior.

2. Materials and methods

2.1. Materials

Polyethyleneimine branched (PEI) (Mw = 25 kDa), iron (III) chloride hexahydrate (≥99%), iron (II) chloride tetrahydrate (98%), polyacrylic acid (PAA, Mw = 1800 kDa), oleic acid (≥90%), potassium dihydrogen phosphate (≥98%), N-hydroxysuccinimide (NHS) (98%), N,N'-dicyclo-hexylcarbodiimide (DCC) (≥99.0%), Poly(ethylene glycol diamine) (NH_2-PEG-NH_2, Mn = 3000), polyvinyl alcohol (PVA, Mowiol 4-88), deuterated chloroform (≥99%), and tetramethylsilane (≥99%) were purchased from Sigma-Aldrich. Dialysis bag (Spectra/Por, MWCO: 3.5 kDa) was purchased from ThermoFisher. Commercial PLGA Mn = 10 kDa (Purasorb PDLG 7502A, 70/30 LA/GA) was kindly donated by Corbion (Gorinchem, Netherlands). Ibuprofen (IBU) was kindly donated by Zentiva group (Prague, Czech Republic). Sodium hydroxide, acetone (p.a 99.5%), acetonitrile, ethyl ether, chloroform, ethanol, ammonia and dichloromethane (DCM) p. a. were purchased from Penta (Prague, Czech Republic). For all experiments, Millipore water was used.

2.2. Synthesis of amine terminated PLGA-PEG-NH_2

The diblock copolymer was synthesized by reaction between the activated PLGA and NH_2-PEG-NH_2 [**28**]. The PLGA carboxyl terminal end group was first activated using NHS and DCC. Briefly, 3 g (0.3 mmol) of PLGA was dissolved in 12 ml of DCM followed by addition of 75 mg (0.65 mmol) of NHS and 138 mg (0.66 mmol) of DCC. The reaction was left under magnetic stirring for 20 h at room temperature. Insoluble dicyclohexyl urea was filtered (Millipore 0.45 μm) and the resultant polymer solution was precipitated using ice-cold diethyl ether. The activated PLGA was completely dried under vacuum at room temperature. The PLGA-NHS ester was conjugated with NH_2-PEG-NH_2 via amide bond. The activated PLGA (2.5 g) was dissolved in 25 ml of DCM with an excess amount of NH_2-PEG-NH_2 (450 mg, 0.15 mmol) and was left under magnetic stirring for 20 h at room temperature. Amine terminated block copolymer was precipitated and washed with ice-cold methanol. The final PLGA-PEG-NH_2 polymer was dried under vacuum at room temperature.

2.3. Production of PEGylated PLGA nanoparticles

Pristine (i.e. PEGylated PLGA) as well as drug loaded PEGylated PLGA (i.e. PEGylated PLGA_IBU) NPs were prepared by nanoprecipitation method described in Zumaya et al. [**15**], with minor modifications. The organic phase containing 100 mg of PLGA-PEG-NH_2, 10 ml acetone and a desired amount of a model drug, i.e. ibuprofen, was stirred until complete dissolution. The ratio of model drug to polymer was set to 1:10 (w/w). Then, the formation of PEGylated PLGA NPs took place by dropwise injection of the organic phase with a flow rate 0.5 ml min^{-1} into 60 ml of the aqueous phase. The aqueous phase was solely pure water. The suspension was stirred overnight at room temperature to allow complete evaporation of acetone. The nanoparticles were purified by washing three times by centrifugation at 14,000 rpm for 45 min at 4 ° C with water. For comparison, drug loaded PLGA NPs were prepared following the same procedure. The final concentration of pristine (i.e. PEGylated PLGA) as well as drug loaded PEGylated PLGA (i.e. PEGylated PLGA_IBU) was set to 1.6 mg/ml.

2.4. Synthesis of iron oxide nanoparticles

The synthesis of two kinds of superparamagnetic IO NPs was performed by the co-precipitation method [**29,30**], i.e. aqueous and organic IO NPs suspensions. PAA and oleic acid (OA) were used as surfactants to prepare IO NPs stabilized in the aqueous (i.e. IO-PAA), and in the organic (i.e. IO-OA) medium, respectively.

The synthesis of IO-PAA was carried out using the protocol described in Zumaya et al. [**15**].

For the synthesis of IO-OA, similar method was used with slight modification. First, 0.98 g (3.70 mmol) of iron (II) chloride tetrahydrate and 2 g (7.40 mmol) of iron (III) chloride hexahydrate were incorporated into 20 ml of degassed Millipore water (30 min of degassing with nitrogen). To initiate the co-precipitation reaction, 8 ml of ammonium hydroxide were added to the mixture by dropwise injection leading to the formation of a dark suspension. Then, 1 g of oleic acid was added to the reaction system, then heated to 80 ° C and stirred for 1 h. Thereafter, the IO suspension was washed by decantation using a strong magnet, followed by washing with water and acetone to remove the excess of oleic acid. The washing step was repeated six times. Finally, the resulting IO-OA NPs were dried in the oven at 40 °C for 24 h and dispersed in chloroform. The final concentration of IO-OA in the suspension was set to 10 mg ml^{-1}.

2.5. Production of drug and iron oxide loaded PEGylated PLGA nanoparticles

The multicomponent loaded PEGylated-PLGA NPs i.e. drug and IO loaded PEGylated PLGA NPs (i.e. PEGylated PLGA_IO-OA_IBU) were produced by single emulsion. The organic phase containing 10 ml of chloroform, 100 mg of PLGA-PEG-NH_2, desired amounts of a model drug (i.e. ibuprofen) and IO-OA NPs suspension, was stirred until complete dissolution of the copolymer and the model drug. The ratio of ibuprofen to PLGA-PEG-NH_2 was set to 1:10 (w/w). Various ratios of IO-OA NPs to polymer were tested. The organic phase was then poured into 20 ml aqueous solution containing 3% (w/w) PVA and emulsified using a sonication probe (Hielscher UP400St) with output power of 40W in pulse mode for 45 min, with on mode for 5 min, followed by off mode for 10 s in an ice bath. The emulsion was then diluted to a final concentration of 1% (w/v) PVA. Finally, the suspension was left under magnetic stirring for 24 h to remove the organic solvent. To wash the NPs, the suspension was centrifuged six times at 14,000 rpm for 45 min at 4 ° C with ultrapure water. The production yield of PEGylated

PLGA_IO-OA_IBU was about 90%. For comparison drug and iron oxide loaded PLGA NPs were prepared under the same conditions. The final concentration of all prepared NPs was set to 2 mg/ml.

2.6. Production of nanoclusters

The production of nanoclusters (i.e. IO-PAA:PEGylated PLGA_IBU) was carried out following the methodology we have developed recently, which is based on self-assembly via electrostatic interactions of oppositely charged polymeric and IO NPs [**15**]. Briefly, each suspension, i.e. 25 ml (2 mg/ml) of drug loaded PEGylated PLGA NPs (i.e. PEGylated PLGA_IBU) and 25 ml (0.68 mg/ml) IO-PAA NPs was dropwise injected at a flow rate of 0.5 ml min^{-1} into a magnetically stirred flask at 100 rpm. The ratio of IO-PAA NPs to drug loaded PEGylated PLGA NPs was set to 1:3 (w/w). The production yield of IO-PAA: PEGylated PLGA_IBU was about 88%.

2.7. Drug loading and dissolution tests

The drug loading was determined by means of UV-Visible spectrophotometer (Agilent Technology, Cary 60). To carry out the measurements, an aliquot of ibuprofen loaded PEGylated PLGA or PLGA suspension was freeze-dried (Freeze Dryer, model Freezone 2,5, Lab-conco (USA)). The resulting powder was dissolved in DMSO to carry out UV-Visible analysis. In the case of the multicomponent PEGylated PLGA NPs, the freeze-dried powder was dissolved in acetonitrile. The concentration of ibuprofen in the polymeric nanoparticles was measured using a calibration curve constructed from absorbance values of known concentrations of ibuprofen solutions in DMSO or in acetonitrile at a wavelength of 264 nm (Figure S1). It is worth mentioning that none of PLGA, PEGylated PLGA and IO-OA NPs interfere with ibuprofen absorbance at this wavelength.

The encapsulation efficiency was calculated as follows:

$$Encapsulation\ efficiency,\ EE\ (\%) = \frac{amount\ of\ encapsulated\ drug}{amount\ of\ drug\ added} * 100$$

In order to carry out the dissolution tests, the suspensions were placed in a dialysis bag (molecular weight cutoff 3.5 kDa) by suspending a weighed amount of nanoparticles in phosphate buffered saline (PBS 0.1 M, pH 7.4). Exactly 20 mg of ibuprofen loaded PEGylated or PLGA NPs was suspended in 2 ml of PBS. The suspensions were then incubated in 50 ml of PBS at 37 °C under magnetic stirring at 100 rpm for 120 h. At specific intervals, 2 ml of sample was withdrawn from the PBS bath and refilled with 2 ml of fresh PBS. The concentration of released ibuprofen as a function of time was monitored using UV-Visible at a wavelength of 264 nm.

2.8. Statistical analysis

All results were expressed as means with standard deviation (n = 3). The statistical analysis of the drug release for all the systems was performed using a one-way ANOVA. Differences between the groups were tested using Student's t-test. All the tests were done with a level of significance as $p \leq 0.05$.

2.9. Characterization

2.9.1. Dynamic light scattering

All drug delivery suspensions (nanoparticles and nanocluster) were analysed using the Zetasizer Nano ZS (Malvern Instruments) to measure their particle size distribution. For each measurement, 1 ml of the suspension in ultrapure water was pipetted into a cuvette without further dilution. DLS measurements were carried out in autocorrelation mode with single illuminating beam and single detector. Each measurement was carried out in triplicate at a scattering angle of 90° at room temperature. Size measurement of the IO-OA NPs was measured using a square glass cuvette in the chloroform media.

2.9.2. Zetasizer potential

Zetasizer Nano ZS (Malvern Instruments) was used to measure the zeta potential of the nanoparticles through the Smoluchowski model. The measurements were performed on 800 µl of ten times diluted aqueous mother suspension. Measurement of zeta potential for the IO-OA NPs was performed by dispersing 28 µL of IO-OA NPs in 1 ml of ultrapure water. The solvent was removed by evaporation and the measurements were performed. It is worth mentioning that IO-OA NPs remained stable in aqueous solution during the measurement.

2.9.3. Transmission Electron Microscopy

The morphology of the IO NPs and nanoclusters was characterized by means of Transmission Electron Microscopy by 100 kV TEM, model JEM-1010 (JEOL, Ltd) equipped with CCD camera MegaView III (Olympus Soft Imaging Systems, Germany). 10 µl of the sample was deposited on a carbon coated electron microscopic grid. The contrasting of the sample was done by water solution of 1% uranyl acetate. The grid was left to dry and then was inserted into the electron microscope column for analysis. Measurements were achieved under 80 kV of accelerating voltage.

2.9.4. Nuclear magnetic resonance

^{1}H NMR analysis were performed on a Bruker Avance III 500-MHz spectrometer. Deuterated chloroform ($CDCl_3$) was used as solvent and tetramethylsilane (TMS) as an internal reference. The ^{1}H NMR spectra were used to determine the ratio of the monomers in the analysed copolymers.

2.9.5. Size Exclusion Chromatography

The mass average molar mass (Mw) and dispersity (D) of the prepared PEGylated PLGA NPs in the drug delivery systems before and after dissolution tests was followed using Size Exclusion Chromatography (SEC) from Agilent liquid chromatograph equipped with an Agilent degasser and differential refractive index detector. The molar mass distributions of the samples were performed in chloroform ($CHCl_3$) at 30 °C at an elution rate of 1 ml min^{-1}. Polystyrene standards were used for calibration.

2.9.6. Vibrating sample magnetometer

The magnetic properties of the drug delivery systems containing IO NPs were assessed using a vibrating sample magnetometer (VSM 7407, Lake Shore, USA) in the presence of the applied magnetic field from —10 kOe to +10 kOe at room temperature.

2.9.7. Fourier-transform infrared spectroscopy

The chemical structure of the multi-component drug delivery systems was examined using a Thermo Scientific Nicolet iS50 FTIR Spectrometer in transmission mode before and after dissolution tests. Pellets containing the freeze-dried samples were prepared with KBr. The spectrum was collected on a 128-scan mode and a resolution of 4 cm^{-1}.

2.9.8. Thermogravimetric analysis

Thermogravimetric analyses (TGA) were carried out to determine the content of iron oxide present in the multi-component drug delivery systems using Stanton-Redcroft TG 750 under air atmosphere (20 ml min^{-1}) from room temperature to 700 °C at a rate of 10 °C min^{-1}.

2.9.9. Differential scanning calorimetry

The Differential Scanning Calorimetry (DSC) analysis were carried out to determine the solid state form (i.e. amorphous or crystalline) of the model drug. The measurements were performed using a Q1000 DSC from TA Instruments, Inc., in the range from — 90 to 100 °C and 50 ml min^{-1} nitrogen gas purge with a heating rate of 10 °C min^{-1}.

3. Results and discussion

3.1. Iron oxide nanoparticles: mean size, surface properties and morphology

IO NPs with narrow particle size distribution (PSD) were obtained by co-precipitation method using two coating agents, i.e. OA and PAA [**29-31**]. Following this procedure, IO-OA NPs dispersed in organic phase and IO-PAA NPs dispersed in aqueous phase were obtained.

The adsorption of the coating agents on the surface of IO NPs was confirmed by FTIR analysis (Figure S2). Indeed, typical peaks of OA in IO-OA NPs at 2923 cm^{-1}, 2852 cm^{-1} and 1710 cm^{-1} corresponding to the asymmetric and symmetric stretching of the methylene groups, and the C=O stretching, respectively, can be noticed [**32**]. Alike, characteristic peaks of PAA in IO-PAA NPs are observed at 1698 cm^{-1} attributed to the C=O stretching and 2855 and 2945 cm^{-1} assigned to sp^3 C-H stretching [**33**].

The size and zeta potential distribution of IO-OA and IO-PAA NPs are shown in Figure S3 and S4 and the mean values are summarized in **Table 1**. As can be seen, the formed IO-OA and IO-PAA NPs exhibit a mean hydrodynamic diameter of 20 ± 4 and 17 ± 5 nm, respectively and a zeta potential of — 36 ± 4 mV and — 35 ± 4 mV, respectively. The zeta potential values indicate that OA as well as PAA adsorbed at the surface of IO NPs acted as effective stabilizers by preventing them from agglomeration. The superparamagnetic magnetite structure, i.e. Fe_3O_4, of both iron oxide nanoparticles was confirmed by XRD analysis (Figure S5 and Table S1), where the distinct peaks at 2θ = 30.1°, 35.5°, 43.2°, 53.5°, 57°

and 62.6°, which is consistent with the conditions of synthesis [**34**]. The average grain size was calculated using Scherrer's equation: $\tau = k\lambda/\beta \cos\theta$ where t is the average grain diameter, κ is the grain shape factor ($\kappa = 0.8$), λ is the incident X-ray wavelength, β is the full width at half-maximum angle of the highest intensity and θ is the corresponding diffraction angle [**35**].

Table 1 Mean particle diameter and zeta potential of the primary nanoparticles and nanoclusters.

Sample name	Mean diameter (nm)[a]	PDI	Zeta Potential (mV)
IO-PAA	17 ± 5	0.265 ± 0.02	−35 ± 4
IO-OA	20 ± 4	0.11 ± 0.06	−36 ± 4
PEGylated PLGA	207 ± 87	0.298 ± 0.05	20 ± 5
PEGylated PLGA_IBU	224 ± 87	0.370 ± 0.03	17 ± 5
IO-PAA:PEGylated PLGA	230 ± 100	0.334 ± 0.01	−17 ± 4
IO-PAA:PEGylated PLGA_IBU	350 ± 71	0.454 ± 0.07	−18 ± 4
PEGylated PLGA_IO-OA	236 ± 85	0.097 ± 0.02	−14 ± 7
PEGylated PLGA_IO-OA_IBU	238 ± 88	0.095 ± 0.02	−10 ± 6
PLGA	143 ± 43	0.025 ± 0.011	−21 ± 6
PLGA_IO-OA_IBU	148 ± 72	0.134 ± 0.048	−20 ± 6

[a]*Mean diameters determined by DLS.*

The average grain size obtained using this equation is about 22 nm for IO-OA NPs and 11 nm for IO-PAA NPs and are comparable to the mean size values obtained by DLS [**15, 36**]. TEM images of both types of IO NPs depicted in **Fig. 1** show their spherical morphology.

It is worth noting that the colloidal stability overtime of the IO NPs evaluated by DLS (Figure S6) indicated that the size of the nanoparticles did not change after a period of two weeks in cold storage conditions. Therefore, owing to their excellent colloidal stability in organic solvents, IO-OA NPs can be encapsulated in a polymeric matrix, i.e. PEGylated PLGA NPs (i.e. PEGylated PLGA_IO-OA). Alike, the excellent stability in water of IO-PAA NPs and their high ionic charge density confer them the potential to be used as a building block to construct drug delivery nanoclusters via electrostatic interactions of oppositely charged nanoparticles.

3.2. Synthesis of PLGA-PEG-NH_2

The formation of PEGylated drug delivery nanoparticles has shown to increase particle stability, prolong their circulation time and reduce intermolecular aggregation when administered in the body [**24,25**]. Therefore, first the copolymer PLGA-PEG-NH_2 was synthesized by activation of PLGA carboxylic end groups with DCC, followed by covalent attachment of NH_2-PEG-NH_2 by conjugation. The reaction procedure is shown in **Scheme 1**.

The chemical structure of PLGA-PEG-NH_2 copolymer was characterized by ^1H NMR and 2D NMR (HMQC). The characteristic peaks for the copolymer based on ^1H NMR are shown in **Fig. 2**. The following signals were assigned as follows: 5.30-5.17 ppm to the -CH- of the lac-tide, 4.90-4.5 ppm to the -CH_2- of the glycolide, 3.61-3.55 ppm to the -CH_2- of the ethylene glycol and at 1.65 ppm to the -CH_3 of lactide, thus confirming the conjugation of PLGA chains with NH_2-PEG-NH_2 [**37**]. The HMQC spectrum (Figure S7) can further confirm the amide bond formed after the conjugation step. The cross peaks falling at 3.67/70.62 ppm ($^1H/^{13}C$) were attributed to the presence of the -CH_2- of the ethylene glycol that provide correlation through the linkage with the carbon at the bond between PLGA and NH_2-PEG-NH_2. A signal at 6.5 ppm (**Fig. 2** inset) showed the presence of amide group between the PLGA and PEG [**37,38**]. Further confirmation of the conjugation with NH_2-PEG-NH_2 was made by FTIR (Figure S2), highlighted by the appearance of a peak at 2881 cm^{-1} (C-H stretching vibration associated to the methylene groups in the PEG chains) [**39,40**].

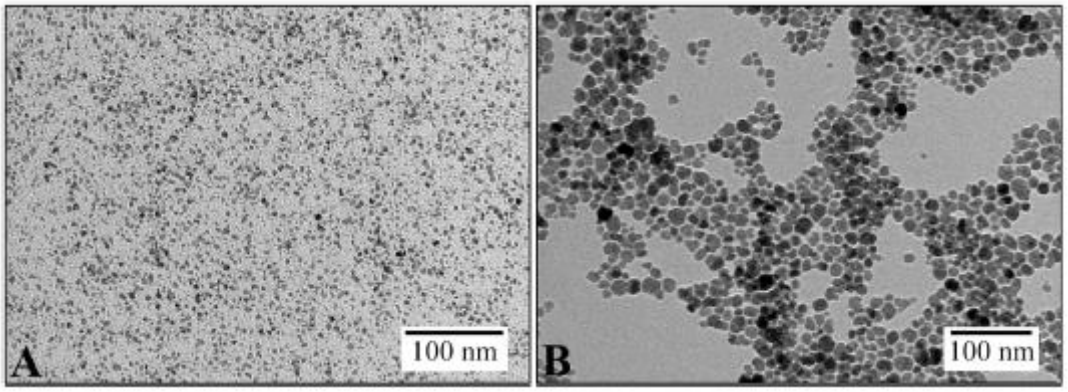

Fig. 1. TEM pictures of A) IO-PAA NPs, and B) IO-OA NPs.

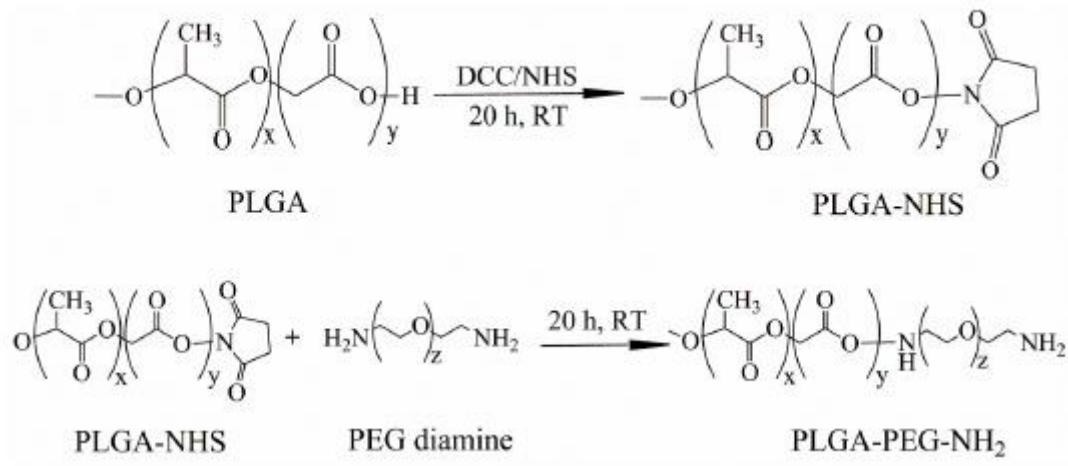

Scheme 1. Synthesis of PLGA-PEG-NH_2 copolymer.

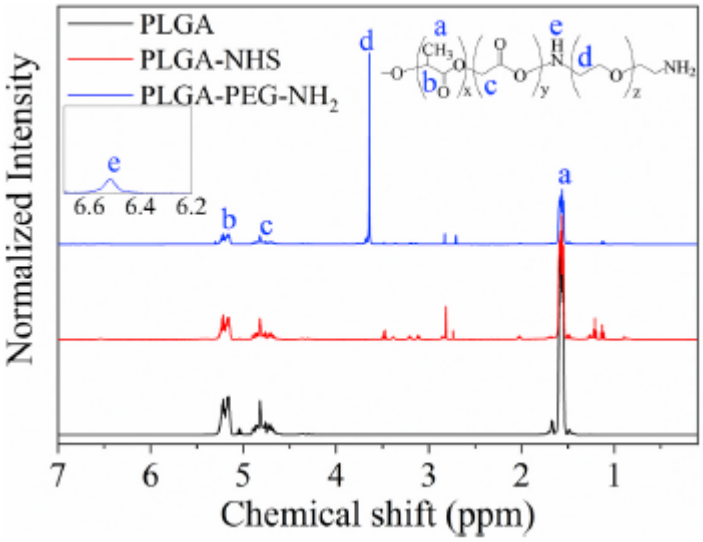

Fig. 2. ^{1}H NMR spectra of PLGA, PLGA-NHS and PLGA-PEG-NH_2.

3.3. Formation of nanoclusters by self-assembly

3.3.1. Mean size and surface properties of the primary PEGylated PLGA NPs

The production of the PEGylated PLGA NPs was achieved by nanoprecipitation method [**15**] following the biomedical recommendations [**4,41,42**]. The size and zeta potential distribution of the nanoparticles measured by DLS are depicted in Figure S3 and S4 and the average values are summarized in **Table 1**. PEGylated PLGA NPs display a mean diameter of 207 ± 87 nm and zeta potential of 20 ± 5 mV. The loading of PEGylated PLGA NPs with ibuprofen, used as a model drug, (i.e. PEGylated PLGA_IBU NPs) with an encapsulation efficiency of 76 ± 3% does not affect the size and the zeta potential of the nanoparticles as a mean diameter of 224 ± 87 nm and zeta potential 17 ± 5 mV were recorded. The free end amine groups of the PEG confer to the surface of the PEGylated PLGA NPs and PEGylated PLGA_IBU NPs with a positive charge at a physiological pH, and introduced ionic charge density to the nanoparticles, needed to construct the drug delivery nanoclusters via electrostatic interactions. In addition, PEG acts as an efficient stabilizer of the nanoparticles.

3.3.2. Formation of nanoclusters

Formation of the nanoclusters by self-assembly of the nanoparticles is usually accomplished by inter-particle interactions such as van der Waals, electrostatic and magnetic interactions. These interactions are intimately dependent on the characteristics of the material composing the nanoparticles, temperature, dielectric constant of solvent, pH and the presence of external stimuli [**43,44**]. The unique attributes of the electrostatic interactions owing to their long-ranging and their attractive or repulsive behavior [**44**], make them suitable for self-assembly of oppositely charged nanoparticles [**45**], with a possibility to tailor their interaction strength and range by changing the charge on the nanoparticles and ionic strength. In our recent work, we have developed a new procedure of preparation of nanoclusters for controlled drug delivery systems in a nanometer size. This approach is based on self-assembly of oppositely charged IO-PAA and PLGA NPs. The nanoclusters were generated by adsorption of IO-PAA NPs at the surface of PLGA NPs through the electrostatic interactions established between the oppositely charged NPs. In particular, it was found out that at a ratio IO-PAA

to PLGA NPs 1:3, a greater control of the assembly kinetics was attained, hence leading to an optimal coverage of PLGA NPs surface by IO-PAA NPs [**15**]. Building on these findings, nanoclusters were prepared by self-assembly of the primary nanoparticles, i.e. positively charged free or drug loaded PEGylated PLGA NPs described above ($\zeta_{\text{PEGylated PLGA NPs}} = 20 \pm 5$ mV. $\zeta_{\text{PEGylated PLGAJBU NPs}} = 17 \pm 5$ mV) and the negatively charged IO-PAA NPs ($\zeta = -35 \pm 4$ mV). The formation of nanoclusters, namely, IO-PAA:PEGylated PLGA and IO-PAA:PEGylated PLGA_IBU in nanometer size of about 230 ± 100 and 350 ± 71 nm, respectively, is attested by the negative values of the zeta potential of −17 ± 4 and −18 ± 4 mV, respectively (**Table 1**), which correspond to the absorption of the IO-PAA NPs on the surface of polymeric nanoparticles via establishment of inter-particle electrostatic interactions [**15**] (**Fig. 3**). The size of the nanoclusters did not evolve after two weeks of cold-storage (~8 °C) (**Fig. 4**), indicating that an equilibrium was reached between the repulsive and attractive forces of the primary nanoparticles, hence reducing their aptitude to agglomeration. In addition, this size, as mentioned above, is correlated with the size of the primary nanoparticles and the ionic strength in the medium [**15**].

3.4. Formation of multicomponent loaded PEGylated PLGA nanoparticles

Besides the nanoclusters, another type of a multicomponent drug delivery system consisting of encapsulation of both model drug (i.e. ibuprofen) and IO NPs into PEGylated PLGA NPs (namely multicomponent loaded PEGylated PLGA NPs) was produced by single emulsion [**46**]. For a sake of understanding of such complex multi-component system, first IO-OA loaded PLGA NPs and IO-OA loaded PEGylated PLGA NPs free of drug were produced by single emulsion. The effect of the ratio IO-OA NPs to polymer (w/w) on the particle size, zeta-potential and encapsulation efficiency was examined on IO-OA loaded PLGA NPs. As depicted in **Fig. 5**, compared to pristine PLGA NPs having an average diameter of 143 ± 43 nm and a zeta potential of − 21 ± 6 mV, IO-OA loaded PLGA NPs prepared with the ratios ranging from 1:10 to 1:100 exhibited comparable average diameter in the range of 146 ± 41 nm as measured by DLS and a comparable zeta potential value of about − 21 ± 5 mV. Hence, the hydrodynamic size of the IO-OA loaded PLGA NPs was not affected by the ratio of IO-OA NPs to polymer. TEM images confirmed this behavior (**Fig. 6**) and image analysis using ImageJ software measured an average diameter size around 99 ± 10 nm, which is in good agreement with DLS measurements. This is in accordance with the literature work, where it was reported that incorporation of magnetite into the polymeric matrix does not affect significantly the final particle size [**47**]. It is worth noting that TEM images highlight also clearly the increase of the IO NPs loading as a function of the ratio IO-OA NPs to polymer from 1:100 to 1:10. At higher IO NPs contents (e.g. ratio IO-OA NPs to polymer 1:5, 1:1) microparticles were formed. Based on these findings, IO-OA loaded PEGylated PLGA NPs were produced from the ratio IO-OA NPs to PLGA-PEG-NH_2 1:10. The IO-OA loaded PEGylated PLGA NPs are characterized by an average diameter of 236 ± 85 nm and a zeta potential of −14 ± 7 mV (**Fig. 5**), which are comparable to those of pristine PEGylated PLGA NPs (i.e. free of IO-OA NPs). When compared to the IO-OA loaded PLGA NPs, IO-OA loaded PEGylated PLGA NPs display higher average diameter, which is associated with the higher molecular weight of the copolymer PLGA-PEG after the conjugation of PLGA chains with NH2-PEG-NH_2 [**48**]. TEM images further confirmed the formation of IO-OA loaded PEGylated PLGA NPs (**Fig. 6**). Interestingly, the IO-OA loaded PEGylated PLGA NPs show a higher clustering of IO-OA NPs within the polymeric matrix than in the case of IO-OA loaded PLGA NPs. This can be explained by the presence of amide and amine groups on PLGA-PEG-NH_2 chains that can establish strong physical interactions via hydrogen bonding with the carboxylic groups from oleic acid [**49**].

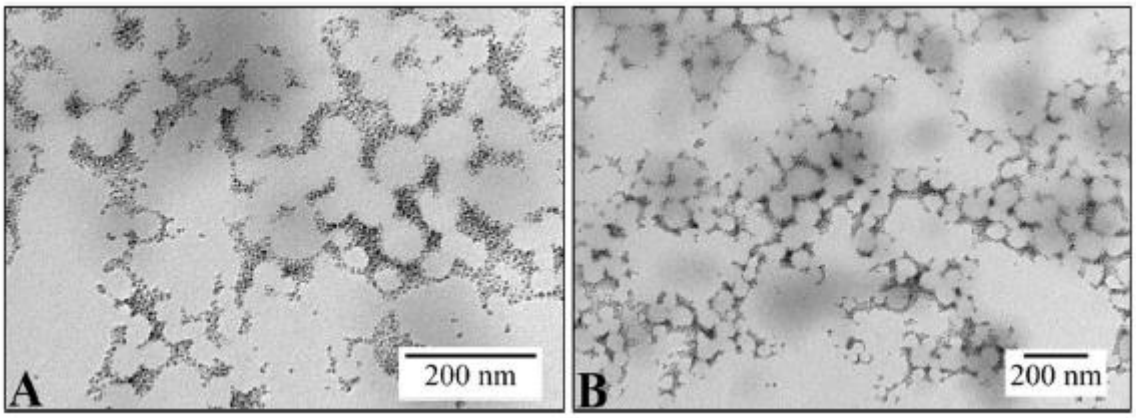

Fig. 3. TEM pictures of the nanoclusters (A) IO-PAA:PEGylated PLGA, and (B) IO-PAA:PEGylated PLGA_IBU.

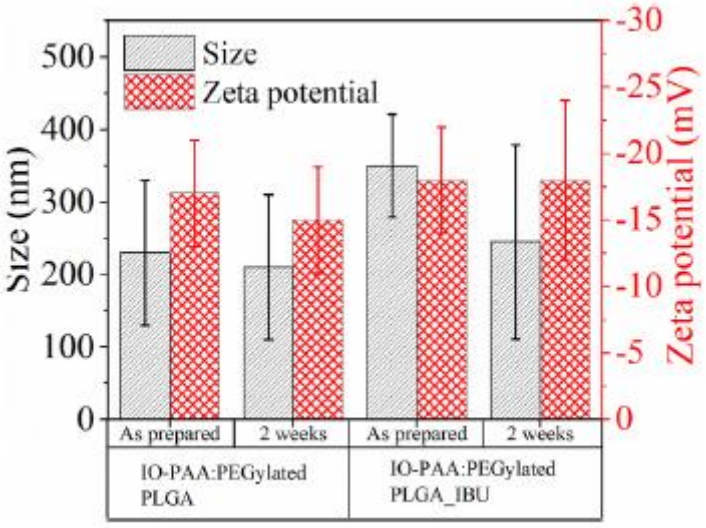

Fig. 4. Size and zeta potential over time of the nanoclusters.

Following the same strategy, IO-OA and ibuprofen loaded PEGylated-PLGA NPs were produced (namely PEGylated PLGA _IO-OA_IBU NPs). The encapsulation of IO-OA NPs into the polymeric matrix was visualized by TEM (**Fig. 6**) and a total content of 6 wt% of iron was determined by TGA (Figure S7), and according to UV-measurements, the PEGylated PLGA NPs possessed a high ibuprofen encapsulation efficiency of about 72 ± 5%. The nanoparticles exhibited an average size of 238 ± 88 nm and a zeta potential of —10 ± 6 mV, (Figure S3 and S4), thus indicating that the size distribution and the surface charge of PEGylated PLGA NPs are not impacted by the loading of ibuprofen and/or IO-OA NPs (**Fig. 5**). The average size distribution depends rather on the sonication power and time, and on the amount of the surfactant [**50**].

For comparison and fundamental understanding of the structure-properties relationships, IO-OA and ibuprofen loaded PLGA NPs were also formulated (namely PLGA_IO-OA_IBU NPs). PLGA_IO-OA_IBU NPs exhibited ibuprofen encapsulation efficiency of 78 ± 6 (**Table 2**) and iron content of 6% (Figure S8), comparable to those PEGylated PLGA_IO-OA_IBU NPs, hence indicating that both ibuprofen and IO-OA NPs are encapsulated at the core of the NPs, namely within PLGA chains.

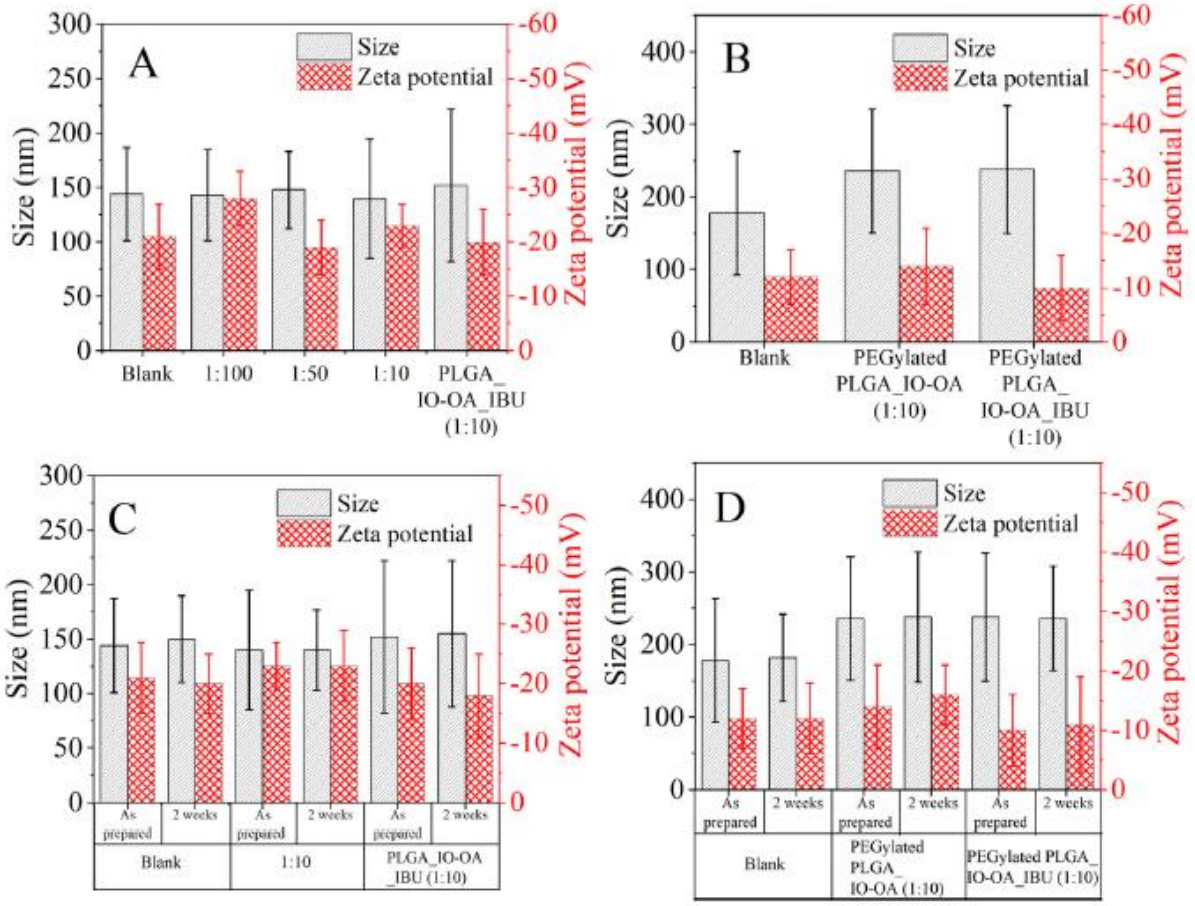

Fig. 5. Mean size and zeta potential of A) PLGA_IO-OA NPs at different ratios IO-OA:PLGA and PLGA_IO-OA_IBU at ratio IO-OA:PLGA equal to 1:10, B) PEGylated PLGA based NPs, C) PLGA based NPs overtime, and D) PEGylated PLGA based NPs overtime. Ratio IO-OA:polymer equal to 1:10 in B), C) and D).

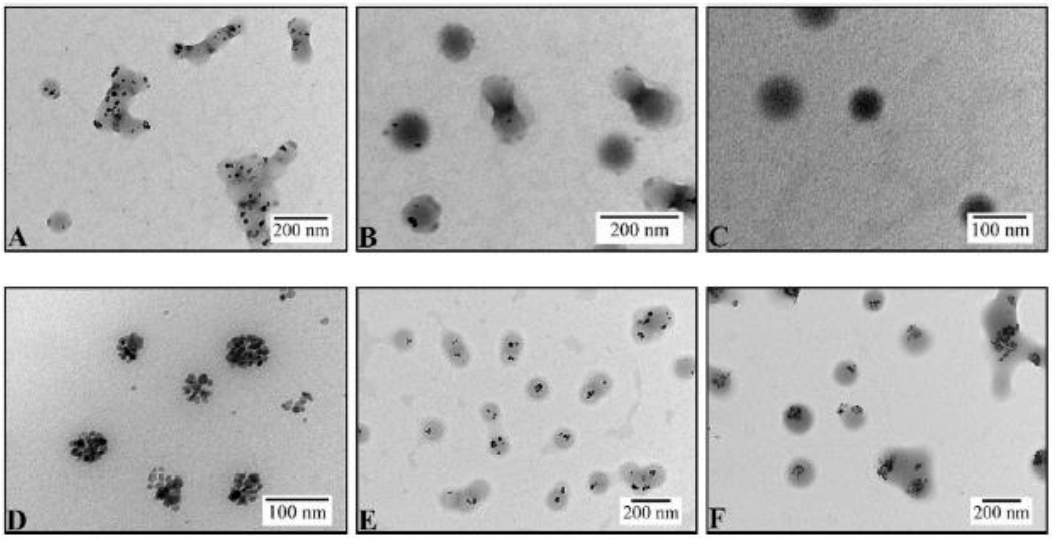

Fig. 6. TEM pictures of A) PLGAJO-OA (Ratio IO-OA:polymer 1:10), B) PLGAJO-OA (Ratio IO-OA:polymer 1:50), C) PLGAJO-OA (Ratio IO-OA:polymer 1:100), D) PEGylated PLGAJO-OA, E) PLGAJO-OAJBU and F) PEGylated PLGAJO-OAJBU NPs. Ratio IO-OA:polymer equal to 1:10 in D), E) and F).

In addition, similarly to PEGylated PLGA_IO-OA_IBU NPs, encapsulation of ibuprofen and IO-OA NPs did not affect the size and the surface charge of PLGA NPs (i.e., average diameter of 148 ± 72 nm and a zeta potential of — 20 ± 6 mV). The formation of PLGA_IO-OA_IBU NPs was further corroborated by TEM (**Fig. 6**). It is important to note the good colloidal stability of the multicomponent loaded PLGA NPs and PEGylated PLGA NPs after two weeks of cold-storage (~8 °C) (**Fig. 5**).

Overall, PEGylation of the PLGA NPs did not have an impact on the encapsulation efficiency of ibuprofen and IO-OA NPs. However, it did affect the size and the zeta potential of the nanoparticles and it is expected to influence the drug release profiles [**6,51,52**].

Table 2 Encapsulation efficiency of ibuprofen in PLGA and PEGylated PLGA NPs

Sample name	Encapsulation efficiency (%)
PLGA_IBU	82 ± 3
PLGA_IO-OA_IBU[a]	78 ± 6
PEGylated PLGA_IBU	75 ± 2
PEGylated PLGA_IO-OA_IBU[a]	72 ± 5

[a]*Ratio IO-OA:polymer equal to 1:10.*

3.5. Dissolution performance and magnetic properties

The performance of the multicomponent drug delivery systems was assessed by the evaluation of their dissolution release profiles and compared to those of their drug loaded polymeric nanoparticles analogs free of IO NPs.

It is worth noting that according to DSC thermograms (Figure S9), ibuprofen encapsulated in both multicomponent drug delivery systems is in an amorphous state as no melting peak corresponding to the drug at 78 °C was detected. Amorphisation of ibuprofen during the particle formation should enhance the bioavailability and thus the dissolution performance of this poorly water soluble drug (class II of Biopharmaceutics Classification System) [**50,53**].

Release profiles of the PLGA_IBU and PLGA_IO-OA_IBU NPs are depicted in **Fig. 7**, where after 3h, an initial burst release of 35 ± 1% and 42 ± 7% is observed, respectively. This is followed by a slower release after 24 h, where the incorporation of IO-OA NPs into the PLGA matrix led to a slightly faster drug release with a cumulative value of 89 ± 6% (i.e. PLGA_IO-OA_IBU) after 120 h while for PLGA_IBU, it reached 79 ± 3%. This result highlights the catalytic effect of IO-OA NPs on the degradation of PLGA matrix ($p \leq 0.05$). As the buffer media comes into contact with PLGA, the hydrolysis of ester bonds takes place leading to lactic and glycolic acid production. The acidic environment is further enhanced by the IO-OA NPs within the matrix thus leading to an autocatalytic process of the hydrolysis [**6,54**]. A similar behavior is observed for the multicomponent loaded PEGylated PLGA_IO-OA NPs, where the incorporation of IO-OA NPs, i.e., PEGylated PLGA_IO-OA_IBU NPs, led to a drug release of 47 ± 6% just after 3 h as compared to the 23 ± 7% of the PEGylated PLGA_IBU NPs. Interestingly, the incorporation of PEG chains into the PLGA matrix also showed an effect on the cumulative drug release as compared to the non-PEGylated PLGA NPs. For instance, the drug loaded PLGA_IBU NPs reached a drug release of 80 ± 3% while the PEGylated PLGA_IBU NPs displayed a cumulative drug release of 94 ± 4% after 120 h. The effect of the hydrophilicity brought by PEG chains facilitated the water uptake and produced a faster drug release [**55**].

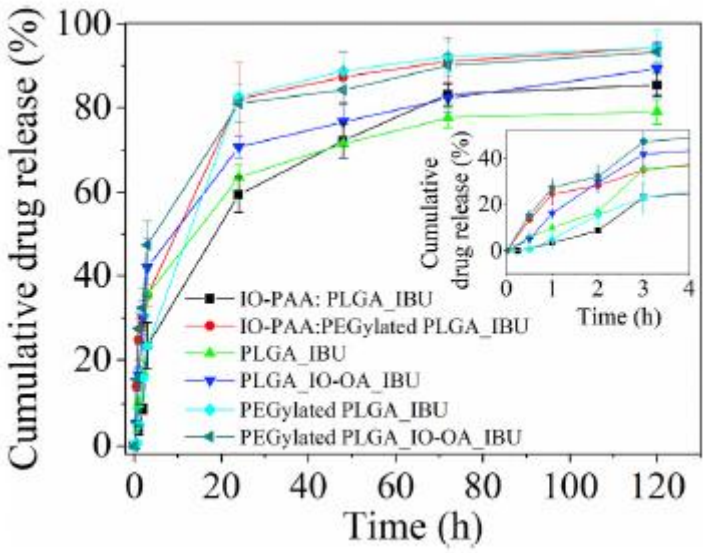

Fig. 7. Drug release profiles of the nanoclusters and the multicomponent loaded PEGylated PLGA nanoparticles over the course of 120 h in PBS at 37 °C, pH 7.4. The IO-PAA:PLGA_IBU was described in our previous work where it was named as IO-PAA:PLGA-PEI_IBU [**15**].

Regarding the nanoclusters, the release profile of IO-PAA:PEGylated PLGA_IBU was examined and compared to that of non-PEGylated PLGA analogs (IO-PAA:PLGA_IBU) [**15**]. According to **Fig. 7**, the non-PEGylated PLGA nanoclusters, namely IO-PAA:PLGA_IBU, exhibited a slower drug release profile (85 ± 3%) in comparison to the IO: PAA-PEGylated PLGA_IBU (94 ± 4%) counterpart after 120 h which can be correlated to the hydrophilic nature of the PEG chains ($p \leq 0.05$). Besides this, interestingly the drug release profile of the PEGylated nanoclusters is quasi-superimposable to that of PEGylated PLGA_IO-OA_IBU NPs, which implies that both multi-component drug delivery systems exhibit similar drug release behavior ($p \geq 0.05$).

A more insightful analysis of the nanoclusters and multicomponent loaded PEGylated PLGA nanoparticles was carried out by means of SEC, TGA and FTIR before and after dissolutions tests in order to understand their drug release mechanisms.

SEC analysis was used to determine the apparent molar mass of the remaining polymer after the dissolution in PBS. According to SEC results summarized in **Table 3**, while the dispersity index (D) remained interestingly quasi-constant in both multicomponent loaded PEGylated PLGA NPs and nanoclusters before and after dissolution experiments, the molar mass (M_n) of the polymeric part of the delivery systems dropped down sharply and drastically after 120 h, i.e., from 12 to 2 and from 12 to 3 kg mol^{-1} for PEGylated PLGA_IO-OA_IBU NPs and IO-PAA: PEGylated PLGA_IBU, respectively. These interesting findings are in agreement with the dissolution tests and confirm that both types of drug delivery systems undergo similar drug release mechanism.

To get insights into the mechanism of degradation of both multicomponent drug delivery systems, FTIR analysis was carried out before and after dissolution tests on the solid fractions.

FTIR spectrum of the nanoclusters IO-PAA:PEGylated PLGA_IBU depicted in Fig. 8A, shows prominent narrow characteristic peaks of PLGA-PEG-NH2 chains (i.e., 1758 cm^{-1}, 1132 cm^{-1} and 1091 cm^{-1}). Besides, a broad band from 3043 cm^{-1} to 3720 cm^{-1} confirms the presence of -OH groups belonging to PLGA-PEG-NH_2 and PAA chains adsorbed on the surface of IO NPs (Figure S2) [**56**]. After dissolution tests, FTIR analysis indicates substantial chemical modifications in the remaining nanoclusters,

highlighted by the appearance of new intense peak at 1600 cm^{-1}, attributed to carboxylate group generated during the hydrolysis process from the formation of acid-amine salt [**57**]. This peak did not appear after dissolution test of the non-PEGylated PLGA nanoclusters reported in our previous work, i.e. IO-PAA:PLGA_IBU [**15**]. This further confirms that the incorporation of a PEG moiety with a primary amine end-groups (-NH_2) in the nanoclusters participates in the formation of amine-acid salt via ionic interactions during the dissolution tests [**58,59**]. The multicomponent loaded PEGylated PLGA_IO-OA_IBU NPs (**Fig. 8B**) has spectral features similar to those of the nanoclusters before as well as after dissolution tests. They suggest that both delivery systems undergo the same mechanism of drug release, which is mainly governed by degradation via hydrolysis of PLGA-PEG-NH_2 chains. Acceleration of the hydrolysis process is caused by hydrophilic nature of PEG and the catalytic effect of the IO NPs [**54,60,61**].

To complete the analysis, TGA measurements were carried out on PEGylated PLGAJO-OAJBU NPs and IO-PAA:PEGylated PLGA_IBU before and after dissolution tests (**Fig. 9** and **Figure S**8).

Table 3 SEC results for the nanoclusters and multicomponent loaded PEGylated PLGA NPs before and after dissolution performance.

Sample name	Mn (kg/mol)	Đ	Mp (kg/mol)[a]
PEGylated PLGA_IO-OA_IBU NPs before	12	1.8	17
PEGylated PLGA _IO-OA_IBU NPs after	2	1.9	3
IO-PAA:PEGylated PLGA_IBU before	12	1.8	17
IO-PAA:PEGylated PLGA_IBU after	3	1.9	3

[a]*Molar mass value at peak maximum.*

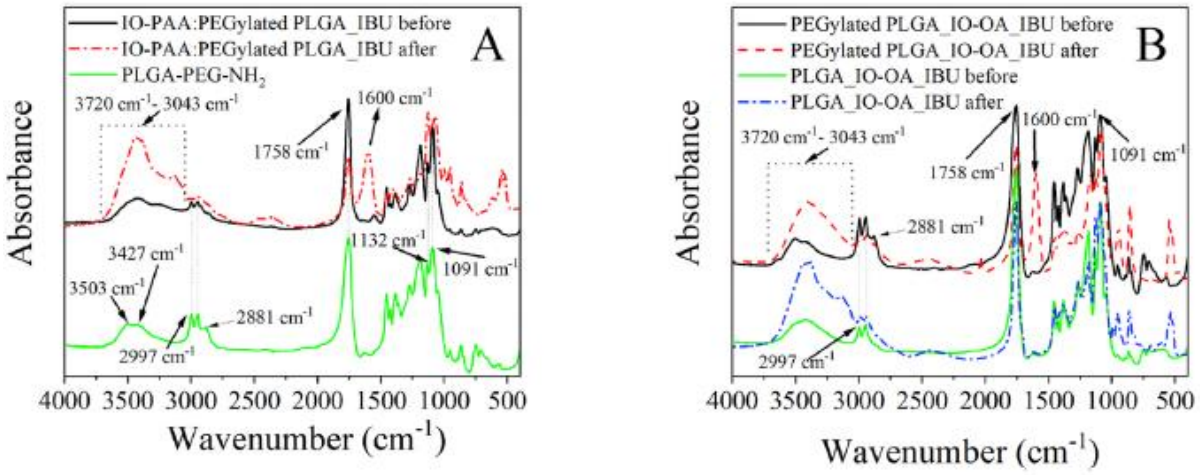

Fig. 8. FTIR spectra of the multicomponent drug delivery systems. (A) IO-PAA:PEGylated PLGA_IBU before, IO-PAA:PEGylated PLGA_IBU after, PLGA-PEG-NH2; (B) PLGAJO-OAJBU before, PLGAJO-OAJBU after, PEGylated PLGAJO-OAJBU before and PEGylated PLGAJO-OAJBU after.

As can be seen in **Fig. 9**, the curve corresponding to the freshly prepared PEGylated PLGAJO-OAJBU NPs reveals a first weight loss of 89% starting at the decomposition onset temperature of 223 °C and ranges to 500 °C and represents the thermal decomposition of the polymeric and organic parts of the nanoparticles (PLGA-PEG-NH_2, PVA and oleic acid surfactants (*Figure S8*)). The remaining solid content of about 6% after thermal decomposition of PEGylated PLGAJO-OAJBU NPs up to 800 °C corresponds

to the iron fraction (without coating) [**20,62**]. In contrast, due to the highly hygroscopic nature of the IO-PAA NPs (Figure S8) **[15]** adsorbed on the surface of PEGylated PLGA NPs in the nanoclusters IO-PAA:PEGylated PLGA_IBU, the latter showed ~10% weight loss from 23 to 150 °C ascribed to moisture evaporation, followed by a significant weight loss of 66% caused by the thermal decomposition of the polymeric part and IO NPs surface coating (i.e., PLGA-PEG-NH2, PAA) in the temperature range 150-544 °C. The remaining weight fraction of 17% recorded at the maximum applied temperature corresponds to the iron content present in the nanoclusters. Unlike in the fresh materials, after dissolution tests both PEGylated PLGAJO-OAJBU NPs and IO-PAA: PEGylated PLGA_IBU exhibited similar thermal behavior [**15**]. The total weight loss of PEGylated PLGAJO-OAJBU NPs and IO-PAA: PEGylated PLGA_IBU up to 800 °C attains 94 and 83%, respectively, before dissolution tests, and 56 and 48%, respectively, after dissolution tests. This clearly demonstrates the presence of higher content of iron in both delivery systems at the end of the dissolution tests (after 120 h) as a result of the degradation of PLGA-PEG-NH_2 chains in PBS at pH 7.4 by hydrolysis (during the dissolution tests).

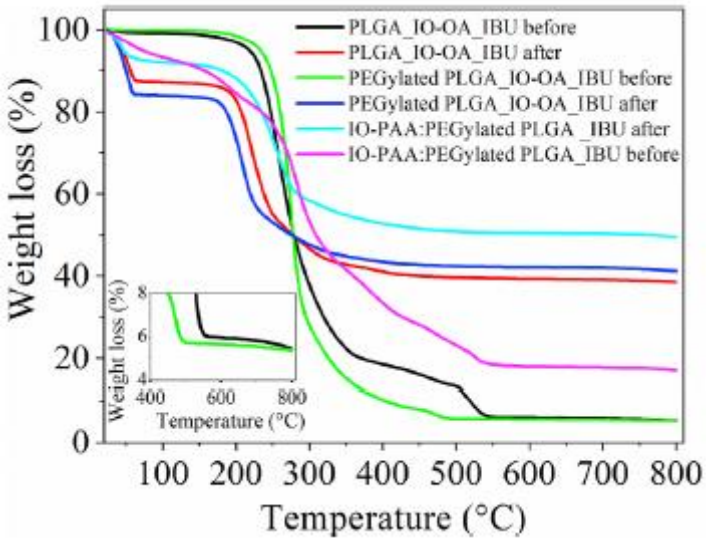

Fig. 9. TG curves for the nanoclusters and multicomponent loaded PEGylated PLGA based nanoparticles before and after dissolution tests.

Hence, based on drug release kinetics, SEC, FTIR and TGA, one can conclude that the location of IO NPs in the drug delivery system, the nature of its coating agent (e.g. PAA, OA) and the method of preparation of the multicomponent delivery system do not affect drug release performance of the material. The drug release mechanism is rather dictated by the chemical composition and the molar mass of the polymeric part of the delivery system.

The magnetic properties of the multicomponent loaded PEGylated PLGA_IO-OA NPs and the nanoclusters assessed before and after dissolution tests are depicted in **Fig. 10**. The nanoclusters exhibited zero remanence on the magnetization and zero coercivity on the magnetization curves. The saturation magnetization values for the freshly prepared IO-PAA:PEGylated PLGA_IBU reach 0.024 emu/g with the coercivity 3.22 Oe. After dissolution test, this value decreased to 0.007 emu/g (coercivity 1.26 Oe). A similar behavior was observed for multicomponent loaded PEGylated PLGAJO-OAJBU NPs (**Fig. 10**), the saturation magnetization values were of 0.022 emu/g and 0.007 emu/g before and after dissolution, respectively. This decrease could be attributed to a partial oxidation of the

magnetite form of IO NPs when exposed for a long period (i.e., 120 h) to PBS buffer [**63**]. The nanoclusters and multicomponent loaded PEGylated PLGA systems exhibit superparamagnetic properties without magnetic hysteresis which makes them suitable for treatment with magnetically mediated hyperthermia, even after drug release [**15**].

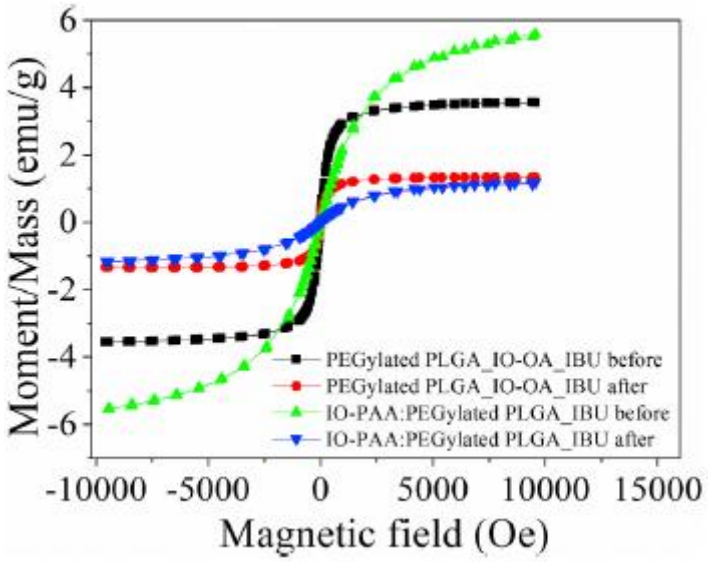

Fig. 10. Magnetization curves for the multicomponent loaded PEGylated PLGA NPs and nanoclusters before and after dissolution tests.

Overall, despite the differences observed between PEGylated PLGA_IO-OA_IBU NPs and IO-PAA:PEGylated PLGA_IBU in terms of size, morphology (localization of IO NPs), zeta potential and the type of coating agent adsorbed on the surface of IO NPs, they exhibited comparable magnetic properties and drug release kinetics, attesting that the mechanism of drug release in both systems is mainly governed by the degradation of the PLGA-PEG-NH2 copolymer by hydrolysis as compared to the non-PEGylated analogs.

4. Conclusions

Two multicomponent and multifunctional drug delivery systems based on PLGA-PEG-NH_2 copolymer were developed and compared in terms of drug release kinetics and magnetic properties. Two approaches based on the assembly of drug loaded PEGylated PLGA NPs and IO NPs were employed for their preparation. In the first approach, preparation of nanoclusters was performed by self-assembly of oppositely charged drug loaded PEGylated-PLGA and IO-PAA NPs, while in the second one IO-OA NPs and a model drug were incorporated inside PEGylated PLGA NPs by single emulsion method. The formed nanoclusters displayed a mean diameter of 350 ± 71 nm and a zeta potential of —18 ± 4 mV. They are formed via a mechanism of adsorption of IO-PAA NPs on the surface of PEGylated PLGA NPs. The multi-component PEGylated PLGA NPs prepared by single emulsion exhibited a mean diameter of 238 ± 88 nm, and a zeta potential of —10 ± 6 mV.

Dissolution tests demonstrated a quasi-superimposed drug release behavior of both delivery systems. Correlation between the drug release profiles, and physico-chemical analysis of the delivery systems before and after dissolution tests (FTIR, TGA and SEC analysis) allowed to identify the effect of

PEGylation and the addition of IO NPs on the mechanism of drug release. They suggest that both delivery systems undergo the same mechanism of drug release via degradation by hydrolysis of PLGA-PEG-NH_2 chains, which is accelerated by the hydrophilic nature of PEG and by the catalytic effect of the IO NPs. In fact, in drug delivery systems based on biodegradable aliphatic polyesters, the mechanism of drug release is governed by the degradation of the polymer mainly by bulk erosion, in which the chains are cleaved by hydrolysis of the ester bonds [**64**]. These results show that the location of IO in the multicomponent delivery system does not affect this mechanism.

The magnetic properties of the multicomponent delivery systems were maintained after dissolution tests though a decrease in the saturation magnetization was observed. This suggests that both delivery systems can be used for magnetically mediated hyperthermia.

Finally, overall this study shows clearly that the location of IO NPs in the drug delivery system, the nature of its coating agent (e.g. PAA, OA) and the method of preparation of the multicomponent delivery system do not affect drug release performance of the material. The drug release mechanism is rather dictated by the chemical composition and the molar mass of the polymeric part of the delivery system.

Both developed multicomponent delivery systems should give the possibility of providing a functional site for surface conjugation of targeting agent and for surface properties improvement, which would enhance their functionalities.

References

[1] T.L. Doane, C. Burda, The unique role of nanoparticles in nanomedicine: imaging, drug delivery and therapy, Chem. Soc. Rev. 41 (7) (2012) 2885-2911.

[2] K. Ulbrich, K. Holá, V. Šubr, A. Bakandritsos, J. Tuček, R. Zbořil, Targeted drug delivery with polymers and magnetic nanoparticles: covalent and noncovalent approaches, release control, and clinical studies, Chem. Rev. 116 (2016) 5338-5431.

[3] C. Boyer, M.R. Whittaker, V. Bulmus, J. Liu, T.P. Davis, The design and utility of polymer-stabilized iron-oxide nanoparticles for nanomedicine applications, NPG Asia Mater. 2 (1) (2010) 23-30.

[4] F. Danhier, E. Ansorena, J.M. Silva, R. Coco, A. Le Breton, V. Préat, PLGA-based nanoparticles: an overview of biomedical applications, J. Contr. Release 161 (2012) 505-522.

[5] A. Kumari, S.K. Yadav, S.C. Yadav, Biodegradable polymeric nanoparticles based drug delivery systems, Colloids Surf. B Biointerfaces 75 (2010) 1-18.

[6] N. Kamaly, B. Yameen, J. Wu, O.C. Farokhzad, Degradable controlled-release polymers and polymeric nanoparticles: mechanisms of controlling drug release, Chem. Rev. 116 (2016) 2602-2663.

[7] M. Nikolaou, A. Pavlopoulou, A.G. Georgakilas, E. Kyrodimos, The challenge of drug resistance in cancer treatment: a current overview, Clin. Exp. Metastasis 35 (4) (2018) 309-318.

[8] C.M. Hu, L. Zhang, Nanoparticle-based combination therapy toward overcoming drug resistance in cancer, Biochem. Pharmacol. 83 (8) (2012) 1104-1111.

[9] F. Ye, Barrefelt A, H. Asem, M. Abedi-Valugerdi, I. El-Serafi, M. Saghafian, et al., Biodegradable polymeric vesicles containing magnetic nanoparticles, quantum dots and anticancer drugs for drug delivery and imaging, Biomaterials 35 (2014) 3885-3894.

[10] Z. Gao, L. Zhang, Y. Sun, Nanotechnology applied to overcome tumor drug resistance, J. Contr. Release 162 (1) (2012) 45-55.

[11] X. Xu, W. Ho, X. Zhang, N. Bertrand, O. Farokhzad, Cancer nanomedicine: from targeted delivery to combination therapy, Trends Mol. Med. 21 (2015) 223-232.

[12] J. Kim, J.E. Lee, S.H. Lee, J.H. Yu, J.H. Lee, T.G. Park, et al., Designed fabrication of a multifunctional polymer nanomedical platform for simultaneous cancer-targeted imaging and magnetically guided drug delivery, Adv. Mater. 20 (2008) 478-483.

[13] H. Danafar, A. Shara fi, S. Askarlou, H.K. Manjili, Preparation and characterization of PEGylated iron oxide-gold nanoparticles for delivery of sulforaphane and curcumin, Drug Res. 67 (12) (2017) 698-704.

[14] P.L. Lam, W.Y. Wong, Z. Bian, C.H. Chui, R. Gambari, Recent advances in green nanoparticulate systems for drug delivery: efficient delivery and safety concern, Nanomedicine 12 (4) (2017) 357-385.

[15] A.L.V. Zumaya, D. Martynek, T. Bautkinova, M. Soás, P. Ulbrich, J.-M. Raquez, et al., Self-assembly of poly(L-lactide-co-glycolide) and magnetic nanoparticles into nanoclusters for controlled drug delivery, Eur. Polym. J. 133 (2020) 109795.

[16] I.S. Smolkova, N.E. Kazantseva, V. Babayan, J. Vilcakova, N. Pizurova, P. Saha, The role of diffusion-controlled growth in the formation of uniform iron oxide nanoparticles with a link to magnetic hyperthermia, Cryst. Growth Des. 17 (5) (2017) 2323-2332.

[17] K. Hola, Z. Markova, G. Zoppellaro, J. Tucek, R. Zboril, Tailored functionalization of iron oxide nanoparticles for MRI, drug delivery, magnetic separation and immobilization of biosubstances, Biotechnol. Adv. 33 (2015) 1162-1176.

[18] E. Attari, H. Nosrati, H. Danafar, H. Kheiri Manjili, Methotrexate anticancer drug delivery to breast cancer cell lines by iron oxide magnetic based nanocarrier, J. Biomed. Mater. Res. 107 (11) (2019) 2492-2500.

[19] Y. Xu, C.S. Kim, D.M. Saylor, D. Koo, Polymer degradation and drug delivery in PLGA-based drug-polymer applications: a review of experiments and theories, J. Biomed. Mater. Res. B Appl. Biomater. 105 (2017) 1692-1716.

[20] C. D'Avila Carvalho Erbetta, Synthesis and characterization of poly(D,L-Lactide-co-Glycolide) copolymer, J. Biomaterials Nanobiotechnol. (2012) 208-225, 03.

[21] E. Locatelli, M. Comes Franchini, Biodegradable PLGA-b-PEG polymeric nanoparticles: synthesis, properties, and nanomedical applications as drug delivery system, J. Nanoparticle Res. 14 (12) (2012).

[22] T. Betancourt, J.D. Byrne, N. Sunaryo, S.W. Crowder, M. Kadapakkam, S. Patel, et al., PEGylation strategies for active targeting of PLA/PLGA nanoparticles, J. Biomed. Mater. Res. 91 (2009) 263-276.

[23] J.V. Jokerst, T. Lobovkina, R.N. Zare, S.S. Gambhir, Nanoparticle PEGylation for imaging and therapy, Nanomedicine 6 (4) (2011) 715-728.

[24] J. Cheng, B.A. Teply, I. Sherifi, J. Sung, G. Luther, F.X. Gu, et al., Formulation of functionalized PLGA-PEG nanoparticles for in vivo targeted drug delivery, Biomaterials 28 (2007) 869-876.

[25] Y.P. Li, Y.Y. Pei, X.Y. Zhang, Z.H. Gu, Z.H. Zhou, W.F. Yuan, et al., PEGylated PLGA nanoparticles as protein carriers: synthesis, preparation and biodistribution in rats, J. Contr. Release 71 (2001) 203-211.

[26] F. Danhier, O. Feron, V. Préat, To exploit the tumor microenvironment : ;passive and active tumor targeting of nanocarriers for anti-cancer drug delivery, J. Contr. Release 148 (2015) 135-146.

[27] Q. Hu, W. Sun, C. Wang, Z. Gu, Recent advances of cocktail chemotherapy by combination drug delivery systems, Adv. Drug Deliv. Rev. 98 (2016) 19-34.

[28] S. Aggarwal, S. Gupta, D. Pabla, R.S.R. Murthy, Gemcitabine-loaded PLGA-PEG immunonanoparticles for targeted chemotherapy of pancreatic cancer, Cancer Nanotechnology 4 (2013) 145-157.

[29] J. Mosafer, K. Abnous, M. Tafaghodi, H. Jafarzadeh, M. Ramezani, Preparation and characterization of uniform-sized PLGA nanospheres encapsulated with oleic acid-coated magnetic-Fe 3 O 4 nanoparticles for simultaneous diagnostic and therapeutic applications, Colloid. Surface. Physicochem. Eng. Aspect. 514 (2017) 146-154.

[30] C.L. Lin, C.F. Lee, W.Y. Chiu, Preparation and properties of poly(acrylic acid) oligomer stabilized superparamagnetic ferrofluid, J. Colloid Interface Sci. 291 (2) (2005) 411-420.

[31] R. Massart, Preparation of aqueous magnetic liquids in alkaline and acidic media, IEEE Trans. Magn. 17 (1981) 1247-1248.

[32] K. Yang, H. Peng, Y. Wen, N. Li, Re-examination of characteristic FTIR spectrum of secondary layer in bilayer oleic acid-coated Fe3O4 nanoparticles, Appl. Surf. Sci. 256 (10) (2010) 3093-3097.

[33] C.W. Liew, H.M. Ng, A. Numan, S. Ramesh, Poly(Acrylic acid)(-)Based hybrid Inorganic(-)Organic electrolytes membrane for electrical double layer capacitors application, Polymers 8 (5) (2016).

[34] D. Maity, D.C. Agrawal, Synthesis of iron oxide nanoparticles under oxidizing environment and their stabilization in aqueous and non-aqueous media, J. Magn. Magn Mater. 308 (2007) 46-55.

[35] P.I.P. Soares, A.M.R. Alves, L.C.J. Pereira, J.T. Coutinho, I.M.M. Ferreira, C.M. M. Novo, et al., Effects of surfactants on the magnetic properties of iron oxide colloids, J. Colloid Interface Sci. 419 (2014) 46-51.

[36] P.I.P. Soares, C.A.T. Laia, A. Carvalho, L.C.J. Pereira, J.T. Coutinho, I.M. M. Ferreira, et al., Iron oxide nanoparticles stabilized with a bilayer of oleic acid for magnetic hyperthermia and MRI applications, Appl. Surf. Sci. 383 (2016) 240-247.

[37] C.W. Liu, W.J. Lin, Polymeric nanoparticles conjugate a novel heptapeptide as an epidermal growth factor receptor-active targeting ligand for doxorubicin, Int. J. Nanomed. 7 (2012) 4749-4767.

[38] S.J. Buwalda, P.J. Dijkstra, L. Calucci, C. Forte, J. Feijen, Influence of amide versus ester linkages on the properties of eight-armed PEG-PLA star block copolymer hydrogels, Biomacromolecules 11 (1) (2010) 224-232.

[39] T.G. Kim, T.G. Park, Surface functionalized electrospun biodegradable nanofibers for immobilization of bioactive molecules, Biotechnol. Prog. 22 (4) (2006) 1108-1113.

[40] Y.H. Lee, D.S. Chang, Fabrication, characterization, and biological evaluation of anti-HER2 indocyanine green-doxorubicin-encapsulated PEG-b-PLGA copolymeric nanoparticles for targeted photochemotherapy of breast cancer cells, Sci. Rep. 7 (2017) 46688.

[41] S. Honary, F. Zahir, Effect of zeta potential on the properties of nano-drug delivery systems - a review (Part 1), Trop. J. Pharmaceut. Res. 12 (2013) 255-264.

[42] A.K. Gupta, M. Gupta, Synthesis and surface engineering of iron oxide nanoparticles for biomedical applications, Biomaterials 26 (2005) 3995-4021.

[43] M. Hans, A. Lowman, Nanoparticles for drug delivery, Nanomaterials Handbook (2006).

[44] K. Singh, A. Raghav, P.K. Jha, S. Satapathi, Effect of size and charge asymmetry on aggregation kinetics of oppositely charged nanoparticles, Sci. Rep. 9 (1) (2019) 3762.

[45] A.M. Kalsin, B. Kowalczyk, S.K. Smoukov, R. Klajn, B.A. Grzybowski, Ionic-like behavior of oppositely charged nanoparticles, J. Am. Chem. Soc. 128 (47) (2006) 15046-15047.

[46] N. Schleich, P. Sibret, P. Danhier, B. Ucakar, S. Laurent, R.N. Muller, et al., Dual anticancer drug/superparamagnetic iron oxide-loaded PLGA-based nanoparticles for cancer therapy and magnetic resonance imaging, Int. J. Pharm. 447 (2013) 94-101.

[47] L. Ngaboni Okassa, H. Marchais, L. Douziech-Eyrolles, S. Cohen-Jonathan, M. Souce, P. Dubois, et al., Development and characterization of sub-micron poly (D,L-lactide-co-glycolide) particles loaded with magnetite/maghemite nanoparticles, Int. J. Pharm. 302 (1-2) (2005) 187-196.

[48] G. Mittal, D.K. Sahana, V. Bhardwaj, M.N. Ravi Kumar, Estradiol loaded PLGA nanoparticles for oral administration: effect of polymer molecular weight and copolymer composition on release behavior in vitro and in vivo, J. Contr. Release 119 (1) (2007) 77-85.

[49] J.S. Parks, D.P. Cistola, D.M. Small, J.A. Hamilton, Interactions of the carboxyl group of oleic acid with bovine serum albumin: a 13C NMR study, J. Biol. Chem. 258 (15) (1983) 9262-9269.

[50] F. Hassouna, M. Abo El Dahab, M. Fulem, A. De Lima Haiek, A. Laachachi, D. Kopecký, et al., Multi-scale analysis of amorphous solid dispersions prepared by freeze drying of ibuprofen loaded acrylic polymer nanoparticles, J. Drug Deliv. Sci. Technol. 53 (2019) 101182.

[51] S. Fredenberg, M. Wahlgren, M. Reslow, A. Axelsson, The mechanisms of drug release in poly(lactic-co-glycolic acid)-based drug delivery systems-a review, Int. J. Pharm. 415 (1-2) (2011) 34-52.

[52] T. Samkange, S. D'Souza, K. Obikeze, A. Dube, Influence of PEGylation on PLGA nanoparticle properties, hydrophobic drug release and interactions with human serum albumin, J. Pharm. Pharmacol. 71 (10) (2019) 1497-1507.

[53] A. Iemtsev, F. Hassouna, A. Mathers, M. Klajmon, M. Dendisové, L. Malinové, et al., Physical stability of hydroxypropyl methylcellulose-based amorphous solid dispersions: experimental and computational study, Int. J. Pharm. 589 (2020) 119845.

[54] B. Mattix, T.R. Olsen, T. Moore, M. Casco, D. Simionescu, R.P. Visconti, et al., Accelerated iron oxide nanoparticle degradation mediated by polyester encapsulation within cellular spheroids, Adv. Funct. Mater. 24 (6) (2014) 800-807.

[55] K. Avgoustakis, A. Beletsi, Z. Panagi, P. Klepetsanis, A.G. Karydas, D.S. Ithakissios, PLGA-mPEG nanoparticles of cisplatin: in vitro nanoparticle degradation, in vitro drug release and in vivo drug residence in blood properties, J. Contr. Release 79 (2002) 123-135.

[56] M.A. Gonzalez-Gomez, S. Belderbos, S. Yanez-Vilar, Y. Pineiro, F. Cleeren, G. Bormans, et al., Development of superparamagnetic nanoparticles coated with polyacrylic acid and aluminum hydroxide as an efficient contrast agent for multimodal imaging, Nanomaterials 9 (11) (2019).

[57] Y. Ji, X. Yang, Z. Ji, L. Zhu, N. Ma, D. Chen, et al., DFT-calculated IR spectrum amide I, II, and III band contributions of N-methylacetamide fine components, ACS Omega 5 (15) (2020) 8572-8578.

[58] K. Avgoustakis, Polylactic-co-glycolic acid (PLGA), Encyclopedia of biomaterials and biomedical engineering 1 (1) (2005) 1-11.

[59] Li S, Vert M. Biodegradation of aliphatic polyesters. In: Scott G, Gilead D, editors. Degradable Polymers1995.

[60] P. Rafiei, A. Haddadi, Docetaxel-loaded PLGA and PLGA-PEG nanoparticles for intravenous application: pharmacokinetics and biodistribution profile, Int. J. Nanomed. 12 (2017) 935-947.

[61] M. Senthilkumar, P. Mishra, N.K. Jain, Long circulating PEGylated poly(D,L-lactide-co-glycolide) nanoparticulate delivery of Docetaxel to solid tumors, J. Drug Target. 16 (5) (2008) 424-435.

[62] Y. Tsuchiya, K. Sumi, Thermal decomposition products of poly(vinyl alcohol), J. Polym. Sci. 1 Polym. Chem. 7 (11) (1969) 3151-3158.

[63] R.L. Rebodos, P.J. Vikesland, Effects of oxidation on the magnetization of nanoparticulate magnetite, Langmuir 26 (22) (2010) 16745-16753.

[64] M. Stankovic, H.W. Frijlink, W.L. Hinrichs, Polymeric formulations for drug release prepared by hot melt extrusion: application and characterization, Drug Discov. Today 20 (7) (2015) 812-823.